Article

# The Formation Mechanism of a Textured Ceramic of Thermoelectric [CaCoO][CoO] on β-Co(OH) Templates through in Situ Topotactic Conversion

Hiroshi Itahara, Won-Seon Seo, Sujeong Lee, Hiroshi Nozaki, Toshihiko Tani, and Kunihito Koumoto

*J. Am. Chem. Soc.*, **2005**, 127 (17), 6367-6373• DOI: 10.1021/ja0434883 • Publication Date (Web): 13 April 2005



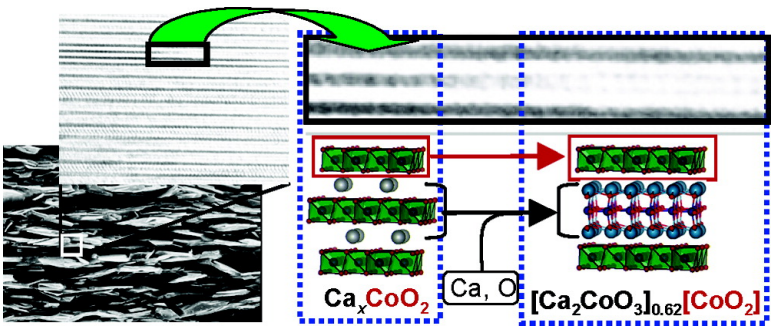


## More About This Article

Additional resources and features associated with this article are available within the HTML version:

- Supporting Information
- Links to the 8 articles that cite this article, as of the time of this article download
- Access to high resolution figures
- Links to articles and content related to this article
- Copyright permission to reproduce figures and/or text from this article

View the Full Text HTML

J|A|C|S
ARTICLES
Published on Web 04/13/2005

# The Formation Mechanism of a Textured Ceramic of Thermoelectric $[Ca_2CoO_3]_{0.62}[CoO_2]$ on $\beta$-$Co(OH)_2$ Templates through in Situ Topotactic Conversion

Hiroshi Itahara,*,† Won-Seon Seo,‡ Sujeong Lee,‡ Hiroshi Nozaki,† Toshihiko Tani,† and Kunihito Koumoto§,||

*Contribution from Toyota Central R&D Laboratories, Inc., Nagakute, Aichi, 480-1192, Japan, Korea Institute of Ceramic Engineering and Technology, Seoul, 153-801, Korea, Graduate School of Engineering, Nagoya University, Nagoya, Aichi, 464-8603, Japan, and CREST-JST, Kawaguchi, Saitama, 332-0012, Japan*

Received October 28, 2004; E-mail: h-itahara@mosk.tytlabs.co.jp

***Abstract:*** We investigated the formation mechanism of thermoelectric $[Ca_2CoO_3]_{0.62}[CoO_2]$ (CCO) on $\beta$-$Co(OH)_2$ templates with maintained orientations by identifying the intermediate phases and specifying the relationship between their crystallographic orientations. We mixed $\beta$-$Co(OH)_2$ templates with the complementary reactant $CaCO_3$ and prepared a compact by tape casting, with the developed (001) plane of the templates aligned along the casting plane. High-temperature XRD of the compact revealed that $\beta$-$Co(OH)_2$ decomposed into $Co_3O_4$ by 873 K, and $Co_3O_4$ reacted with CaO to form CCO by 1193 K via the formation of the newly detected intermediate phase $\beta$-$Na_xCoO_2$-type $Ca_xCoO_2$ at 913−973 K. Pole figure measurements and SEM and TEM observations revealed that the relationship between the crystallographic planes was (001) $\beta$-$Co(OH)_2$//{111} $Co_3O_4$//(001) $Ca_xCoO_2$//(001) CCO. The crystal structures of the four materials possess the common $CoO_2$ layer (or similar), which is composed of edge-sharing $CoO_6$ octahedra, parallel to the planes. The cross-sectional HRTEM analysis of an incompletely reacted specimen showed transient lattice images from $Ca_xCoO_2$ into CCO, in which every other $CoO_2$ layer of $Ca_xCoO_2$ was preserved. Thus, it was demonstrated that a textured CCO ceramic is produced through a series of in situ topotactic conversion reactions with a preserved $CoO_2$ layer of its template.

## Introduction

Fabrication of textured ceramics is one of the effective means for enhancing mechanical properties (e.g., fracture toughness and bending strength) and physical properties (e.g., thermoelectric, piezoelectric, ferroelectric, and magnetic properties) of functional ceramics. For instance, textured ceramics have been widely prepared by the "oriented consolidation of anisotropic particles (OCAP) method"[1−3] and templated grain growth (TGG)[4−7] method, using single crystalline particles with anisotropic (platelike or needlelike) shape. These textured ceramics showed unique or enhanced properties when compared to nontextured ceramics prepared by conventional sintering.

However, these methods are applicable to a limited number of material systems because of the compositional limitation imposed by the synthesis of single-crystal particles. To overcome this disadvantage, we extended the fabrication strategy exploited in the topotactic synthesis of a textured Mn−Zn ferrite ceramic[8] and proposed the reactive-templated grain growth (RTGG) method.[9] The basic concept is (1) to find a reactive template material (a reactive seed) having a simple composition and lattice matching with a target material, (2) to design a topotactic reaction between the template and its complementary reactants, and (3) to synthesize in situ the target material, which preserves crystallographic orientation of the reactive template. The RTGG method enables us to fabricate textured ceramics for various substances.[9−18] For instance, a textured ceramic of piezoelectric

† Toyota Central R&D Laboratories, Inc.
‡ Korea Institute of Ceramic Engineering and Technology.
§ Nagoya University.
|| CREST-JST.

(1) Granahan, M.; Holmes, M.; Schulze, W. A.; Newnham, R. E. *J. Am. Ceram. Soc*. **1981**, *64*, C68.
(2) Kimura, T.; Holmes, M.; Newnham, R. E. *J. Am. Ceram. Soc*. **1982**, *65*, 223.
(3) Watanabe, H.; Kimura, T.; Yamaguchi, T. *J. Am. Ceram. Soc*. **1989**, *72*, 289.
(4) Hirao, K.; Ohashi, M.; Brito, M. E.; Kanzaki, S. *J. Am. Ceram. Soc*. **1995**, *78*, 1687.
(5) Seabaugh, M. M.; Kerscht, I. H.; Messing, G. L. *J. Am. Ceram. Soc*. **1997**, *80*, 1181.
(6) Hong, S.-H.; Messing, G. L. *J. Am. Ceram. Soc*. **1999**, *82*, 867.
(7) Sabolsky, E. M.; Messing, G. L.; Trolier-McKinstry, S. *J. Am. Ceram. Soc*. **2001**, *84*, 2507.
(8) Hirota, E.; Kugimiya, K.; Nishio, T. *J. Jpn. Soc. Powder Powder Metall.* **1979**, *26*, 123.
(9) Tani, T. *J. Korean Phys. Soc*. **1998**, *32*, S1217.
(10) Masuda, Y.; Nagahama, D.; Itahara, H.; Tani, T.; Seo, W.-S.; Koumoto, K. *J. Mater. Chem*. **2003**, *13*, 1094.
(11) Itahara, H.; Fujita, K.; Sugiyama, J.; Nakamura, K.; Tani, T. *J. Ceram. Soc. Jpn*. **2003**, *111*, 227.
(12) Takeuchi, T.; Tani, T.; Saito, Y. *Jpn. J. Appl. Phys*. **1999**, *38*, 5553.
(13) Tani, T.; Takeuchi, T.; Seno, Y. *Ceram. Trans*. **2000**, *104*, 267.
(14) Fukuchi, E.; Kimura, T.; Tani, T.; Takeuch, T.; Saito, Y. *J. Am. Ceram. Soc*. **2002**, *85*, 1461.
(15) Tani, T.; Isobe, S.; Seo, W.-S.; Koumoto, K. *J. Mater. Chem*. **2001**, *11*, 2324.
(16) Tajima, S.; Tani, T.; Isobe, S.; Koumoto, K. *Mater. Sci. Eng*. **2001**, *B86*, 20.

10.1021/ja0434883 CCC: $25.25 

$Bi_{0.5}(Na,K)_{0.5}TiO_3$ (simple perovskite-type structure) was prepared by using $Bi_4Ti_3O_{12}$ (layered perovskite structure) as a reactive template.[9] In particular, even if a reactive template has only a partial similarity in the crystal structure to a target substance, the RTGG method is applicable to the production of a textured ceramic: By using $\beta$-$Co(OH)_2$ template particles,[19] we have prepared textured ceramics[20−22] with enhanced thermoelectric properties for various layered cobaltites, such as $[Ca_2CoO_3]_{0.62}[CoO_2]$[23−25] (abbreviated to CCO), $[Ca_2(Co_{0.65}Cu_{0.35})_2O_4]_{0.624}[CoO_2]$,[26] and $[Bi_2M_{2-x}O_4]_p[CoO_2]$ (M = Sr[27,28] or Ca[29]), where $\beta$-$Co(OH)_2$ is composed of an edge-sharing $CoO_6$ octahedra layer similar to the $CoO_2$ sublattice layer of cobaltites. The degree of orientation of RTGG-processed layered cobaltite ceramics showed, however, considerable dependence on composition: the degree of orientation of $[Bi_2Sr_{2-x}O_4]_p[CoO_2]$ ceramic was clearly lower than those of other layered cobaltite ceramics containing Ca in their crystal structures.[22]

While the RTGG method is a powerful technique, it was reported[30] that a metastable intermediate phase could disturb the succession of texture from template to target material when the intermediate phase does not share common crystallographic features with the template and target material. Thus, the formation mechanism of any target material must be investigated on different template for the achievement of the fabrication of highly textured ceramics with desired compositions. In the case of the above-mentioned $Bi_{0.5}(Na,K)_{0.5}TiO_3$ ceramic, an electron microscopic analysis indicated that a simple perovskite-type material was formed on the $Bi_4Ti_3O_{12}$ template with preserved ⟨001⟩ orientations.[31] On the other hand, the formation mechanism of textured cobaltite ceramics has not been fully investigated. In previous reports,[20,21] we deduced that a textured ceramic is formed by the topotactic conversion of (001) $\beta$-$Co(OH)_2$ → {111} $Co_3O_4$ → (001) CCO since all three materials possess edge-sharing octahedral $CoO_2$ layers (or similar) parallel to the planes. In addition, our deduction was supported by the result[32] that the degree of preferred (001) orientation of CCO ceramics increases with increasing degree of preferred (001) orientation of the $\beta$-$Co(OH)_2$ templates before their decomposition into $Co_3O_4$.

This article elucidates the formation mechanisms of a textured CCO ceramic by identifying the intermediate phases and the relationships between their crystallographic orientations. We conducted thermal and structural analyses on RTGG-processed specimens during in situ formation reactions. We must design and fabricate layered cobaltite ceramics with optimum compositions as well as a highly preferred orientation because the modulation of electronic structure of the $CoO_2$ layer, by coordinating the composition and structure of the block layer ($Ca_2CoO_3$ layer in CCO), would determine the intrinsic thermoelectric properties.[33] Thus, we believe that investigating the conversion mechanism is extremely important for development of bulk cobaltite ceramics with high thermoelectric properties.

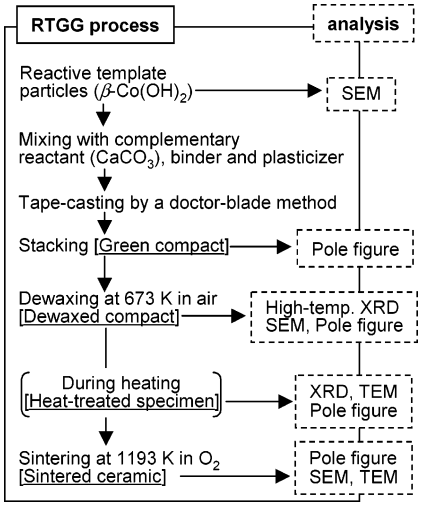


***Figure 1.*** Schematic flowchart of the RTGG process using $\beta$-$Co(OH)_2$ templates for the fabrication of a textured CCO ceramic and analytical methods used for the clarification of the formation mechanism of a textured CCO ceramic on a $\beta$-$Co(OH)_2$ template with maintained preferred orientations.

## Experimental Section

Figure 1 shows the standard processing flowchart for a textured CCO ceramic.[20,21] We used precipitation-prepared $\beta$-$Co(OH)_2$ platelets (average diameter: ∼0.5 $\mu$m; thickness: ∼0.1 $\mu$m)[19] as reactive templates. The templates were mixed with the complementary reactant ($CaCO_3$: Ube Material Industries, Ltd.; particle size: ∼0.2 $\mu$m), polyvinyl butyral (binder, Sekisui Chemical Co. Ltd.), and di-*n*-butyl phthalate (plasticizer, Wako Pure Chemical Industries Ltd.) in an ethanol−toluene solution (ethanol/toluene = 4:6, Wako Pure Chemical Industries). We set the nominal composition to Ca/Co = 3.0:3.92 according to the reported crystal structure of CCO.[25] The mixed slurry was tape-cast by a doctor-blade technique, and the obtained sheet (∼100-$\mu$m thick) was dried in air at room temperature, cut, and stacked to form a monolithic plate (green compact) with ∼3-mm thickness. The organic compounds in the green compact were dewaxed at 673 K in air (dewaxed compact) before the final heat treatment for in situ synthesis and densification of CCO. Table 1 summarizes the specimen preparation conditions and analytical methods used for investigating the formation mechanism of a textured CCO ceramic that maintained the orientation of its templates.

Transition of crystalline phases for the compounds in an RTGG-processed specimen during heat treatment was determined by high-temperature X-ray diffraction (XRD) (model Rint TTR II, Rigaku Co., Cu Kα radiation). The XRD measurement was carried out on a surface parallel to the casting plane of the dewaxed compact (DWC) after heating (10 K/min) up to 673, 913, 973, 1103, and 1163 K in air flow of ∼5 $dm^3$/min. To determine the formation of an intermediate phase, if any, we also measured powder XRD patterns for quenched and crushed specimens after heat treatment at 973 K in $O_2$ flow

(17) Sugawara, T.; Nomura, Y.; Kimura, T.; Tani, T. *J. Ceram. Soc. Jpn.* **2001**, *109*, 897.
(18) Takeuchi, T.; Tani, T. *J. Ceram. Soc. Jpn.* **2002**, *110*, 232.
(19) Itahara, H.; Tajima, S.; Tani, T. *J. Ceram. Soc. Jpn.* **2002**, *110*, 1048.
(20) Tani, T.; Itahara, H.; Xia, C.; Sugiyama, J. *J. Mater. Chem.* **2003**, *13*, 1865.
(21) Itahara, H.; Xia, C.; Seno, Y.; Sugiyama, J.; Tani, T.; Koumoto, K. *Proc. 22nd Int. Conf. Thermoelectr. (ICT2003)*; Hérault, France, Aug 17−21, 2003; IEEE: Piscataway, 2004; p 188.
(22) Itahara, H.; Xia, C.; Sugiyama, J.; Tani, T. *J. Mater. Chem.* **2004**, *14*, 61.
(23) Li, S.; Funahashi, R.; Matsubara, I.; Ueno, K.; Yamada, H. *J. Mater. Chem.* **1999**, *9*, 1659.
(24) Masset, A. C.; Michel, C.; Maignan, A.; Hervieu, M.; Toulemonde, O.; Studer, F.; Raveau, B.; Hejtmanek, J. *Phys. Rev. B* **2000**, *62*, 166.
(25) Miyazaki, Y.; Onoda, M.; Oku, T.; Kikuchi, M.; Ishii, Y.; Ono, Y.; Morii, Y.; Kajitani, T. *J. Phys. Soc. Jpn.* **2002**, *71*, 491.
(26) Miyazaki, Y.; Miura, T.; Ono, Y.; Kajitani, T. *Jpn. J. Appl. Phys.* **2002**, *41*, L849.
(27) Funahashi, R.; Matsubara, I.; Sodeoka, S. *Appl. Phys. Lett.* **2000**, *76*, 2385.
(28) Leligny, H.; Grebille, D.; Pérez, O.; Masset, A. C.; Hervieu, M.; Raveau, B. *Acta Crystallogr.* **2000**, *B56*, 173.
(29) Maignan, A.; Hébert, S.; Hervieu, M.; Michel, C.; Pelloquin, D.; Khomskii, D. *J. Phys.: Condens. Matter* **2003**, *15*, 2711.
(30) Takeushi, T.; Tani, T. *Key Eng. Mater.* **2002**, *216*, 3.
(31) Seno, Y.; Tani, T. *Ferroelectrics* **1999**, *224*, 365.
(32) Itahara, H.; Sugiyama, J.; Tani, T. *Jpn. J. Appl. Phys.* **2004**, *43*, 5134.
(33) Sugiyama, J.; Brewer, J. H.; Ansaldo, E. J.; Itahara, H.; Tani, T.; Mikami, M.; Mori, Y.; Sasaki, T.; Hébert, S.; Maignan, A. *Phys. Rev. Lett.* **2004**, *92*, 017602.

***Table 1.*** Descriptions and Preparation Conditions of the Specimens Used for the Analysis of the Formation Mechanism of a Textured CCO ($[Ca_2CoO_3]_{0.62}[CoO_2]$) Ceramic

| analysis | specimen | characteristics (preparation conditions) |
|---|---|---|
| high-temp XRD | DWC | dewaxed compact (673 K, air) |
| powder XRD | HTP-1 | heat-treated powder (973 K, $O_2$ flow, 10 min, quenched) |
| | HTP-2 | heat-treated powder (973 K, $O_2$ flow, 30 min, quenched) |
| | HTP-3 | heat-treated powder (973 K, $O_2$ flow, 2 h, quenched) |
| pole figure | GRN | green body |
| | DWC | dewaxed compact (973 K, $O_2$ flow, 10 min) |
| | HTC-1 | heat-treated compact (973 K, $O_2$ flow, 10 min) |
| | STC-1 | sintered ceramic (1193 K, $O_2$ flow, 8 h) |
| SEM | $\beta$-$Co(OH)_2$ | $\beta$-$Co(OH)_2$ platelets |
| | DWC | dewaxed compact (673 K, air) |
| | STC-2 | sintered ceramic (1193 K, $O_2$, uniaxial pressing of 19.6 MPa, 20 h) |
| TEM | HTC-2 | heat-treated compact (1043 K, $O_2$, uniaxial pressing of 9.8 MPa, 15 min) |
| | HTC-3 | heat-treated compact (1073 K, $O_2$, uniaxial pressing of 9.8 MPa, 15 min) |
| | STC-2 | sintered ceramic (1193 K, $O_2$, uniaxial pressing of 19.6 MPa, 20h) |

(250 mL/min) for 10 min (the specimen, HTP-1), 30 min (HTP-2), and 2 h (HTP-3). To determine the crystal structure of the intermediate phase, we performed Rietveld analysis using RIETAN-2000[34] on the XRD pattern obtained for HTP-1.

We conducted pole figure (PF) measurements for a green compact (GRN), a DWC, a heat-treated specimen, and a sintered ceramic specimen to determine the preferred orientations of Co-containing substances encountered during processing. Here, the specimens were heat-treated and sintered, respectively, at 973 K in $O_2$ flow (250 mL/min) for 10 min (specimen HTC-1) and at 1193 K in $O_2$ flow (250 mL/min) for 8 h (STC-1). PF was obtained for the surface parallel to the casting plane of the specimens in terms of the planes parallel to the common $CoO_2$ layer in the crystal structures of the Co-containing substances. In these measurements, azimuthal ($\beta$, $0° < \beta < 360°$) scans were carried out in a reflection geometry around the normal direction of the above plane at various polar angles ($\alpha$, $0° < \alpha < 75°$) with constant incident ($\theta$) and diffraction ($2\theta$) angles corresponding to the plane. We evaluated the "preferred orientation function" for the normal direction of these planes ($F_{ND}$).[35]

The morphology of $\beta$-$Co(OH)_2$ templates was observed using scanning electron microscopy (SEM, model Sigma-V, Akashi, Ltd.). The microstructural observations by SEM were performed for the fracture surface of the DWC and sintered ceramic specimen (STC-2). Here, the STC-2 was prepared by sintering at 1193 K in $O_2$ atmosphere with uniaxial pressing at 19.6 MPa for 20 h.

To confirm that CCO forms via an intermediate phase with preserved crystallographic orientations, electron diffraction and chemical analysis of the heat-treated specimens were conducted using an electron microscope (JEM 4010, JEOL, Ltd.) operated at 400 kV, equipped with an EDS (Oxford Link ISIS system). Cross-sectional specimens were prepared by mechanical grinding and polishing, followed by Ar ion-milling, which is the final thinning step in making the specimen electron-transparent using $Ar^+$ ions excited at a voltage of 3 keV and directed toward the specimen at an angle of 4°. For the observations, RTGG-processed dewaxed specimens were heat-treated under conditions ensuring that the reaction would stop short of completion: heat treatment at 1043 K (specimen HTC-2) or 1073 K (HTC-3) in $O_2$ atmosphere with uniaxial pressing at 9.8 MPa for 15 min. In addition, we studied TEM images of the sintered ceramic specimen (STC-2), in which the formation of CCO had proceeded to completion.

## Results and Discussion

Figure 2 shows the high-temperature XRD results obtained for DWC, which was found to be a mixture of $Co_3O_4$ and $CaCO_3$ (Figure 2a). The decomposition of $\beta$-$Co(OH)_2$ (the reactive template) into $Co_3O_4$ was corroborated also by the

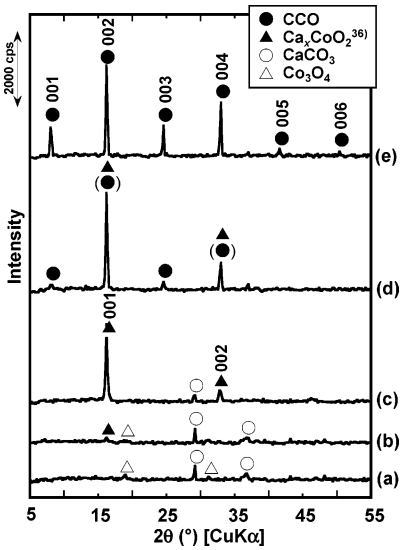


***Figure 2.*** Results of high-temperature XRD for a surface parallel to the casting plane of a DWC during heating in air flow. Measured at (a) 673, (b) 913, (c) 973, (d) 1103, and (e) 1163 K. CCO represents $[Ca_2CoO_3]_{0.62}$-$[CoO_2]$.

results of thermogravimetry and differential thermal (TG-DTA) and powder XRD analyses (see Figures S1 and S2 in Supporting Information). At 913−973 K, the CaO (a product of $CaCO_3$ decomposition) is considered to react with $Co_3O_4$ to form an intermediate phase (Figure 2b,c). The XRD pattern for the intermediate phase is found to be similar to that of the layer-structured $Ca_{0.5}[CoO]_2$[36,37] (hereafter called $Ca_xCoO_2$), which comprises alternating Ca cation and $CoO_2$ layers. $Ca_xCoO_2$ was expected to react with residual CaO at 1103−1163 K to form CCO, where all the XRD peaks for the specimen heated at 1163 K were assigned to CCO (Figure 2d,e).

To confirm $Ca_xCoO_2$ formation prior to CCO formation, we measured powder XRD patterns (Figure 3) for isothermally heated (at 973 K) and quenched specimens (HTP-1, HTP-2, and HTP-3). First, diffraction peaks assigned to $Ca_xCoO_2$ were detected in addition to those from $CaCO_3$ and $Co_3O_4$ for HTP-1 (Figure 3a). After being heated for 30 min (HTP-2 specimen), diffraction peaks assigned to CCO appeared besides those from

(34) Izumi, F.; Ikeda, T. *Mater. Sci. Forum* **2000**, *321−324*, 198.
(35) Hermans, P. H.; Platzek, P. *Kolloid-Z.* **1939**, *88*, 68.
(36) Miyazaki et al. Tohoku University, 2004; Private communication to be submitted for publication: Yuzuru Miyazaki et al. have determined the crystallographic data of $Ca_xCoO_2$ by using its single crystal; triclinic, with $a = 4.924(2)$ Å, $b = 5.683(3)$ Å, $c = 5.685(3)$ Å, $\alpha = 75.400(9)°$, $\beta = 89.974(9)°$, and $\gamma = 81.261(9)°$.
(37) Cushing, B. L.; Wiley, J. B. *J. Solid State Chem.* **1998**, *141*, 385.

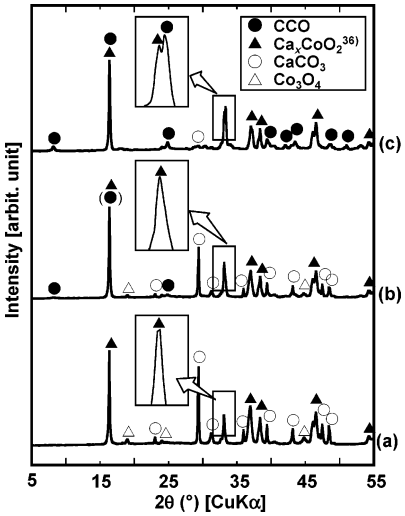


***Figure 3.*** XRD patterns for crashed specimens after heat treatment at 973 K in $O_2$ flow for (a) 10 min (HTP-1 specimen), (b) 30 min (HTP-2), and (c) 2 h (HTP-3). CCO represents $[Ca_2CoO_3]_{0.62}[CoO_2]$.

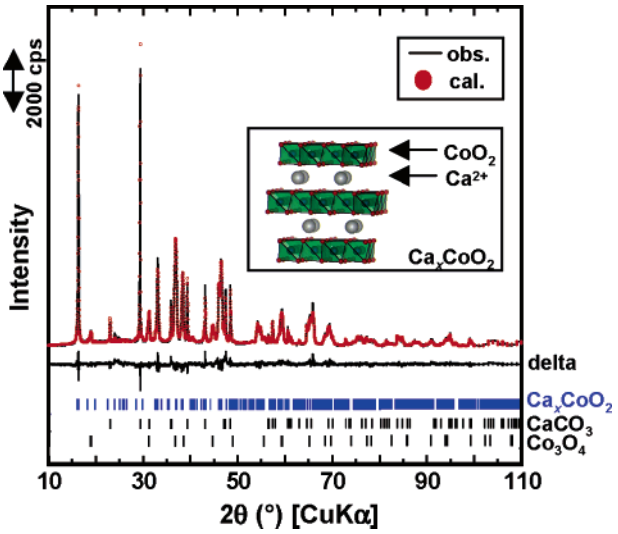


***Figure 4.*** Comparison of the observed XRD pattern of the HTC-1 specimen and the calculated XRD pattern by Rietveld analysis. Inset shows the schematic representation of the model structure of $Ca_xCoO_2$. Delta shows the difference of intensities between measured and calculated XRD patterns.

$CaCO_3$ and $Co_3O_4$ (Figure 3b). Finally, both the number and strength of the CCO peaks increased while the $Co_3O_4$ peaks disappeared in HTP-3 specimen heated for 2 h (Figure 3c). Thus, it was confirmed that CCO was formed via the formation of the intermediate phase, $Ca_xCoO_2$.

To determine the crystal structure of $Ca_xCoO_2$, we performed Rietveld analysis (Figure 4) on the XRD pattern of the heat-treated specimen (HTP-1), which consisted of $Ca_xCoO_2$, $Co_3O_4$, and $CaCO_3$. The background was eliminated, and pseudo-Voight function was used for the analysis. We used the atomic positions in the space group (*P1*, triclinic) for $Ca_xCoO_2$,[36] which were determined by using single crystalline $Ca_xCoO_2$ particles, in which $Ca_xCoO_2$ is shown[36] to have a $\beta$-$Na_xCoO_2$-type structure[38] with $CoO_2$ layer (composed of edge-sharing $CoO_6$ octahedra) and Ca cations stacked alternately (see the inset in Figure 4).

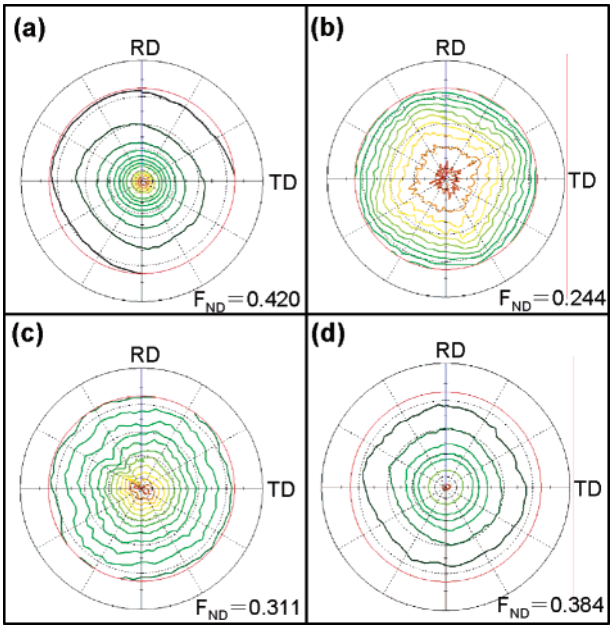


***Figure 5.*** Results of PF measurements for the (a) (001) plane of $\beta$-$Co(OH)_2$ templates in a GRN, (b) (111) plane of $Co_3O_4$ in a DWC, (c) (001) plane of $Ca_xCoO_2$ in a heat-treated compact (HTC-1), and (d) (002) plane of CCO in a sintered ceramic (STC-1). $F_{ND}$ represents the value of the preferred orientation function evaluated in the normal direction[35] of the measured plane.

For both the peak positions and intensities of $Ca_xCoO_2$, the calculated XRD pattern was in good agreement with the measured XRD pattern. The reliability factors were $R_{wp}$ = 8.89%, $R_e$ = 5.00%, $s$ = 1.78, $R_I(Ca_xCoO_2)$ = 3.61%, $R_I(CaCO_3)$ = 7.29%, and $R_I(Co_3O_4)$ = 4.28%. In addition, the lattice parameters for $Ca_xCoO_2$ derived from the analysis (triclinic, $a$ = 4.9072(4) Å, $b$ = 5.6661(3) Å, $c$ = 5.6637(4) Å, $\alpha$ = 75.293(7)°, $\beta$ = 89.981(9)°, $\gamma$ = 80.969(5)°) were close enough to those reported for a $Ca_xCoO_2$ single crystal.[36] The calculated mass percentages of the compounds were 50.96, 19.69, and 29.36 wt % for $Ca_xCoO_2$, $Co_3O_4$, and $CaCO_3$, respectively.

PF measurements (Figure 5) indicate that the (001), (111), (001), and (002) planes, respectively, of $\beta$-$Co(OH)_2$ in GRN, $Co_3O_4$ in DWC, $Ca_xCoO_2$ in HTC-1, and CCO in STC-1 were aligned parallel to the casting plane: the contours of the diffraction intensity from these planes were concentrated at the pole, and $F_{ND}$ values were those for substantially oriented specimens ($F_{ND}$ = 0.0 for completely random and $F_{ND}$ = 1.0 for perfectly oriented). These results suggest that the crystallographic planes were in the relationship of (001) $\beta$-$Co(OH)_2$// {111} $Co_3O_4$//(001) $Ca_xCoO_2$//(001) CCO.

An SEM photograph of the $\beta$-$Co(OH)_2$ templates (Figure 6a) reveals them to be hexagonal platelets. According to oriented particulate monolayer XRD measurements,[39] the developed plane of the templates was the (001) plane[21] (the inset of Figure 6a). The SEM photograph of the DWC (Figure 6b) indicates that $Co_3O_4$ particles maintained the hexagonal platelike morphology of the templates and that the developed plane of the $Co_3O_4$ particles was along the casting plane. These results suggest that the (001) plane of $\beta$-$Co(OH)_2$ templates is converted into the {111} plane of $Co_3O_4$ particles, which is consistent

(38) Fouassier, C.; Matejka, G.; Reau, J.-M.; Hagenmuller, P. *J. Solid State Chem.* **1973**, *6*, 532.

(39) Sugimoto, T.; Muramatsu, A.; Sakata, K.; Shindo, D. *J. Colloid Interface Sci.* **1993**, *158*, 420.

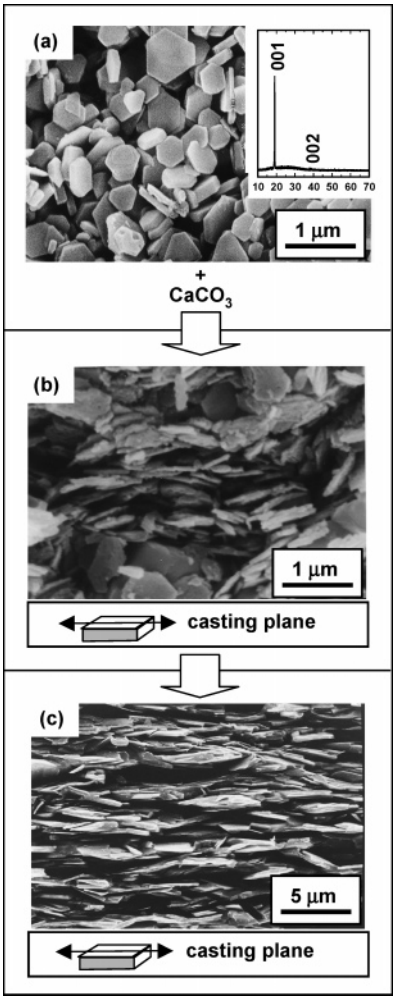


***Figure 6.*** SEM photographs for (a) $\beta$-$Co(OH)_2$ templates (inset shows the oriented particulate monolayer XRD[39] pattern obtained for $\beta$-$Co(OH)_2$[21]), (b) a fracture surface perpendicular to the casting plane of a DWC, and (c) a fracture surface perpendicular to the casting plane of a sintered ceramic (STC-2).

with the PF results (Figure 5a,b). The conversion is in agreement with the topotactic relationship between the crystal structures. $\beta$-$Co(OH)_2$ is composed of edge-sharing $CoO_6$ octahedra layers along the (001) plane. In $Co_3O_4$, on the other hand, there are two different layers along the {111} plane: one composed of the $CoO_6$ octahedra and the other is a mixed layer of $CoO_6$ octahedra and $CoO_4$ tetrahedra. Finally, an SEM photograph (Figure 6c) and PF measurement of the (002) plane (Figure 5d) of sintered ceramic specimens suggest that the developed plane of CCO grains was (001) and parallel to the casting plane.

Figure 7 shows a high-resolution TEM (HRTEM) image and the selected area electron diffraction (SAED) pattern for STC-2 in which the formation of CCO had proceeded to completion. It was found that the ED pattern corresponded to CCO crystal structure. According to the simulated HRTEM image of CCO,[40] the dark linear contrast is derived from the $CoO_2$ layer of CCO, and the three arrays of the dark spots are due to the triplicate rock salt-type structure of CCO.

Figure 8 represents the cross-sectional HRTEM image of HTC-2. The figure shows the structural transition from $Co_3O_4$

(40) Seo, W.-S.; Lee, S.; Lee, Y.; Lee, M.-H.; Masuda, Y.; Koumoto, K. *J. Electron Microsc.* **2004**, *53*, 397.

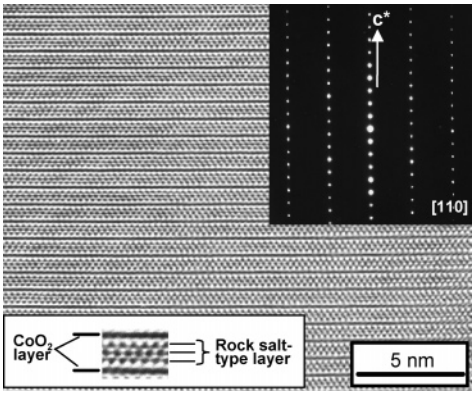


***Figure 7.*** Cross-sectional HRTEM image and SAED pattern of the sintered ceramic (STC-2). The image and diffraction pattern were taken with the incident beam parallel to the [110] direction in the unit cell for a $Ca_2CoO_3$ block of CCO. The inset shows the simulated HRTEM image[40] of CCO containing alternating $CoO_2$ and rock salt-type layers.

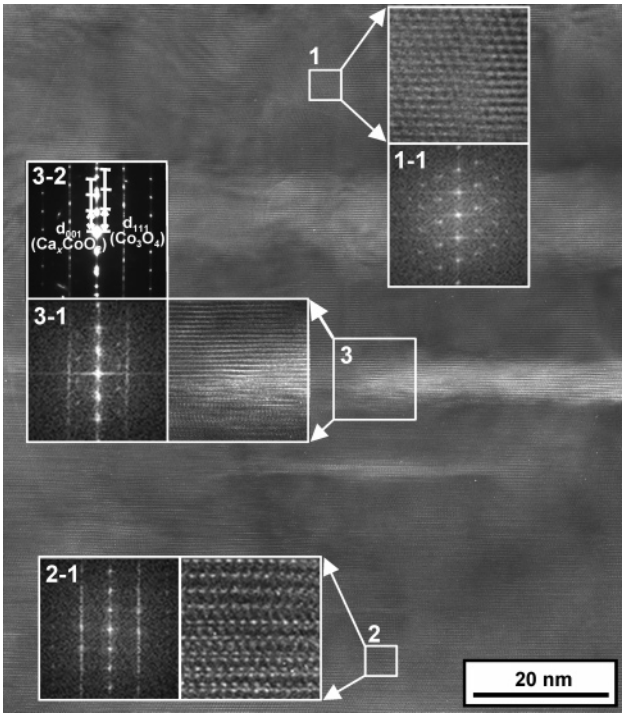


***Figure 8.*** FFTs (designated as 1−1, 2−1, and 3−1) of the corresponding cross-sectional HRTEM image of the heat-treated specimen (HTC-2), which were numbered as 1, 2, and 3, show the structural transition from $Co_3O_4$ (region designated as number 1) to $Ca_xCoO_2$ (region designated as number 2). SAED (designated as 3−2) was taken from the middle part, wider region than for FFT filtering, and exhibited the crystallographic orientation relation between $Co_3O_4$ and $Ca_xCoO_2$.

(region marked 1) to $Ca_xCoO_2$ (region marked 2) by SAED patterns and fast Fourier transform (FFT) images. The FFT of region 1 indicated the characteristic hexagonal network of reflection intensities for the {111} plane of $Co_3O_4$. In addition, EDS analysis revealed the ratio of Ca/Co (atom %) to be less than 0.06 in the upper part of region 1. The FFT image of the selected region (i.e., region 2) exhibited a layered structure. The Ca/Co ratio (atom %) was found to be ∼0.4 by EDS analysis, which pointed toward the $Ca_xCoO_2$ structure as well. On the other hand, the crystallographic orientation relationship between $Co_3O_4$ and $Ca_xCoO_2$ was clearly identified in the SAED (designated as 3−2), which was taken from the middle part of

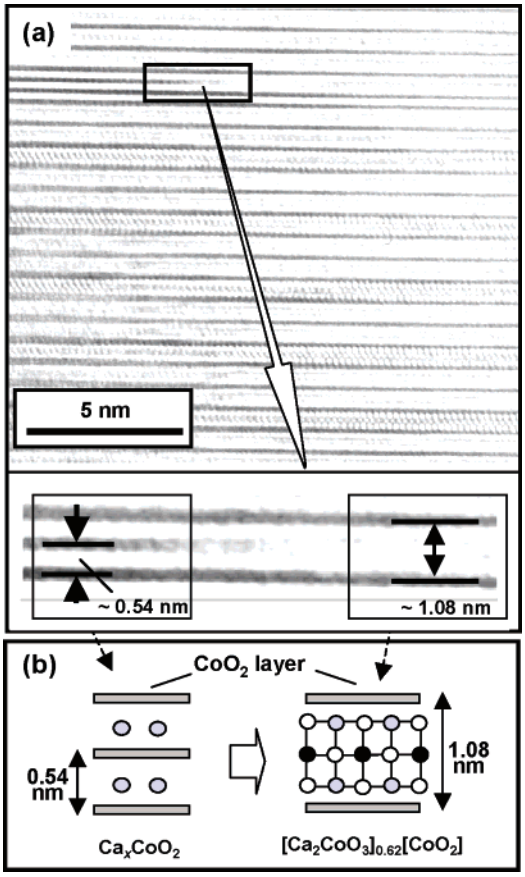


***Figure 9.*** (a) Cross-sectional HRTEM image of the heat-treated specimen (HTC-3). The image was taken with the incident beam parallel to the [110] direction in the unit cell for a $Ca_2CoO_3$ block of CCO. (b) Schematic representation of the possible interpretation for the observed contrasts shown in the magnified view for a part of the TEM image.

the image. The (001) plane of $Ca_xCoO_2$ was shown to be exactly parallel to the {111} plane of $Co_3O_4$. The *d* spacings of the (001) plane for $Ca_xCoO_2$ and the (111) plane for $Co_3O_4$ were calculated to be 0.551 and 0.462 nm, respectively. The diffraction pattern for $Co_3O_4$ overlapped with that of $Ca_xCoO_2$ in the FFT image (designated as 3−1). In addition to these patterns, the epitaxial relationship observed at the boundary of the $Ca_xCoO_2$ and $Co_3O_4$ phases (part 3) supports the crystallographic relationship {111} $Co_3O_4$//(001) $Ca_xCoO_2$ revealed by PF measurements (Figure 5b,c). It is considered that Ca and O would diffuse into the $Co_3O_4$ structure without perturbing the frameworks of the $CoO_6$ octahedra during the formation of $Ca_xCoO_2$ with preserved orientation. This is expected by the analogy to the following two phenomena: (1) Li cations are intercalated and deintercalated between $CoO_2$ layers in the $Li_xCoO_2$ cathode during the charge and discharge process, respectively, and (2) Ca cations enter between $CoO_2$ layers during the synthesis of $Ca_xCoO_2$ by the ion exchange of $Na_xCoO_2$.[37]

Figure 9a gives an HRTEM image of HTC-3 prepared by heat treatment at a temperature (1073 K) higher than that for the HTC-2 (1043 K). It is observed that three successive dark lines spaced ~0.54 nm apart are gradually transformed into the two dark lines aligned at ~1.08-nm intervals, with bright and dark contrasts between them. Here, the dark line corresponds to the $CoO_2$ layer, according to the simulated HRTEM image shown in the inset of Figure 7. In the magnified figure in Figure 9a, the image on the left-hand side is expected to correspond to $Ca_xCoO_2$ judging by the intervals of the adjacent dark linear contrasts that indicate the $CoO_2$ layer. On the other hand, the image on the right-hand side presumably corresponds to a CCO-like structure because of the similarity of the spacing of the linear contrasts indicating the $CoO_2$ layer even though the spots due to the rock salt-type layer between the linear contrasts are less evident when compared to those of CCO shown in Figure 7. Here, in the case of CCO, the projected potentials of a column of Ca and Co atoms are represented by the dark spots, which reflect the electrostatic potential maxima, because all Ca and Co atoms in unit cells in the rock-salt type layer ($Ca_2CoO_3$ blocks) are positioned exactly on top of each column in the [110] direction. In addition, bright spots situated between the dark spots correspond to electrostatic potential minima, that is, empty channels between constituent atoms in the structure. Therefore, the image with the unclear spots would be derived from the CCO-like structure, in which the formation of the rock-salt type layer was nearly completed. The interpretation that the image is of a CCO-like structure is corroborated also by an HRTEM image of a different section of the HTC-3 specimen in Figure 9 (see Figure S4 in Supporting Information), which indicates the presence of Ca-deficient CCO before CCO formation was completed. It was found that the linear arrays of the spots (indicating the rock salt-type layer of CCO) between the dark linear contrast (indicating $CoO_2$ layer of CCO) were evident in some part, while the spots were not distinctive in the other part. EDS analysis indicates that the amount of Ca in the latter part (Ca/Co = 0.5−0.65) was smaller than that of nominal composition of CCO (Ca/Co = 3:3.92). On the other hand, the $d_{001}$ value of the latter part was close enough to that of CCO. Thus, the possible interpretation of Figure 9a is that $Ca_xCoO_2$ provided a part of $CoO_2$ layers to form the $CoO_2$ layer of CCO, while the other $CoO_2$ layers reacted with Ca and O to form the rock salt-type layer of CCO (Figure 9b).

Figure 10 schematizes the crystal structures of $CdI_2$-type $\beta$-$Co(OH)_2$, spinel-type $Co_3O_4$, $\beta$-$Na_xCoO_2$-type $Ca_xCoO_2$, and the misfit-layer-structured CCO, which are topotactically related: There are $CoO_2$ layers composed of edge-sharing $CoO_6$ octahedra along the (001) plane in the case of $\beta$-$Co(OH)_2$, $Ca_xCoO_2$, and CCO and along the {111} plane in the case of $Co_3O_4$. As described above, it is considered that a textured CCO ceramic is formed by in situ topotactic conversion of (001) $\beta$-$Co(OH)_2$ → {111} $Co_3O_4$ → (001) $Ca_xCoO_2$ → (001) CCO, where the $\beta$-$Co(OH)_2$ template provides the $CoO_2$ layer, the common framework of the crystal structures. This formation mechanism is also supported by the previous result that the degree of orientation of CCO increased with increasing degree of orientation of the $\beta$-$Co(OH)_2$ templates.[32] The intermediate $Ca_xCoO_2$ phase might play a key role in the topotactic formation of misfit-layered cobaltites containing Ca from $\beta$-$Co(OH)_2$ template since Ca-free $[Bi_2Sr_{2-x}O_4]_p[CoO_2]$ did not give highly textured ceramics by the RTGG method using the same $\beta$-$Co(OH)_2$ template as the other layered cobaltites.[22] The current study represented the first evidence that topotactic conversion is essential for texture development on templates with maintained orientations.

## Conclusions

We investigated the formation mechanism of a textured CCO ceramic during the RTGG process using a $\beta$-$Co(OH)_2$ template

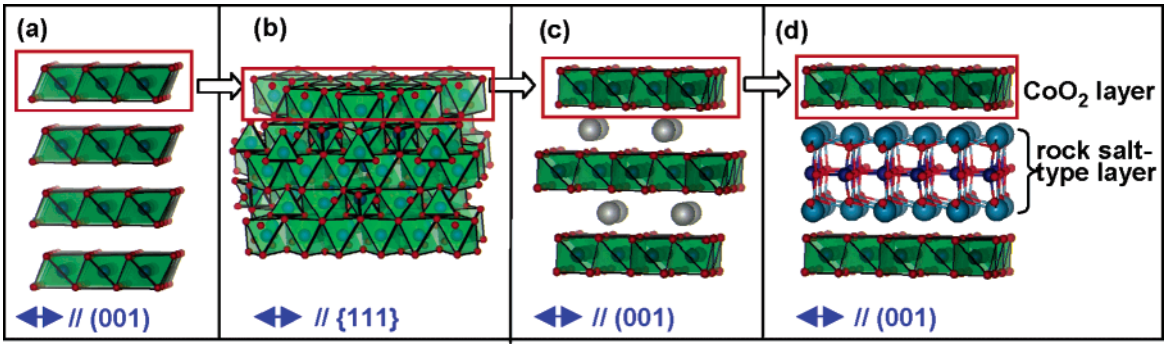


***Figure 10.*** Schematic representations for the crystal structures of (a) $CdI_2$-type $\beta$-$Co(OH)_2$, (b) spinel-type $Co_3O_4$, (c) $\beta$-$Na_xCoO_2$-type $Ca_xCoO_2$, and (d) misfit-layer-structured CCO, with topotaxial relationship with one another.

and the complementary reactant, $CaCO_3$. High-temperature XRD measurements showed that $Co_3O_4$ and CaO, derived, respectively, from the decomposition of $\beta$-$Co(OH)_2$ and $CaCO_3$, reacted to form the intermediate $Ca_xCoO_2$ phase, and finally $Ca_xCoO_2$ reacted with the residual CaO to form CCO. Reitveld analysis indicated that $Ca_xCoO_2$ has a $\beta$-$Na_xCoO_2$-type layered structure with alternately stacked $CoO_2$ layers and Ca cations. PF measurements revealed the relationship between the crystallographic planes: (001) $\beta$-$Co(OH)_2$//{111} $Co_3O_4$//(001) $Ca_xCoO_2$//(001) CCO. This was also supported by the following results: (1) SEM observations showed that the hexagonal shape of (001)-plane-developed $\beta$-$Co(OH)_2$ particles was maintained for $Co_3O_4$ particles with preferred {111} plane in a dewaxed compact. (2) TEM observations of specimens subjected to an incomplete heat treatment revealed that adjacent $Ca_xCoO_2$ and $Co_3O_4$ particles have an epitaxial relationship and that the common $CoO_2$ layer is preserved in the transient lattice image from $Ca_xCoO_2$ to CCO. Thus, it has been proven, for the first time, that $\beta$-$Co(OH)_2$ templates provide the $CoO_2$ layer of CCO via $Co_3O_4$ and $Ca_xCoO_2$ during the topotactic formation of a textured CCO ceramic with maintained preferred orientation. In general, the current article emphasizes the importance of a reaction design in which crystallographic similarities from the starting material all the way through the target substance must be at least partially maintained during the fabrication scheme of highly textured polycrystals with enhanced physical properties.

**Acknowledgment.** We thank Dr. Yuzuru Miyazaki of Tohoku University for giving us structural information on $Ca_{0.5}[CoO_2]$. We are grateful to Dr. Kayo Horibuchi, Dr. Yoshiki Seno, Dr. Jun Sugiyama, and Dr. Ryoji Asahi of Toyota CRDL for fruitful discussions on the formation mechanisms of CCO. The crystal structures shown in Figures 4 and 10 were drawn with VENUS developed by Dr. Ruben Dilanian and Dr. Fujio Izumi of National Institute for Materials Science. This work was partly carried out by joint research and development with International Center for Environmental Technology Transfer in 2002−2004, commissioned by the Ministry of Economy Trade and Industry.

**Supporting Information Available:** Figure S1: Results of powder XRD for (a) precipitation-prepared template particles and (b) the particles obtained after the templates were heat-treated at 973 K in air. Figure S2: Results of TG-DTA analysis (air flow, 10 K/min) for $\beta$-$Co(OH)_2$ templates. Figure S3: Results of TG-DTA analysis (air flow, 10 K/min) of a crashed powder of a dewaxed compact (DWP) composed of $Co_3O_4$ and $CaCO_3$. Figure S4: Cross-sectional HRTEM image and SAED pattern of the heat-treated specimen (HTC-3), showing (1) CCO and (2) Ca-deficient CCO. The image and diffraction pattern were taken with the incident beam parallel to the [110] direction in the unit cell for a $Ca_2CoO_3$ block of CCO. This material is available free of charge via the Internet at http://pubs.acs.org.

JA0434883